

Difference-frequency generation in an AlGaAs Bragg-reflection waveguide using an on-chip electrically-pumped quantum dot laser

A. Schlager,^{1,*} M. Götsch,¹ R. J. Chapman,¹ S. Frick,¹ H. Thiel,¹ H. Suchomel,² M. Kamp,² S. Höfling,^{2,3} C. Schneider,^{2,4} and G. Weihs¹

¹*Institut für Experimentalphysik, Universität Innsbruck, Technikerstraße 25, 6020 Innsbruck, Austria*

²*Technische Physik, Universität Würzburg, Am Hubland, 97074 Würzburg, Germany*

³*School of Physics & Astronomy, University of St Andrews, St Andrews KY16 9SS, UK*

⁴*Institute of Physics, University of Oldenburg, D-26129 Oldenburg, Germany*

(Dated: February 19, 2021)

Nonlinear frequency conversion is ubiquitous in laser engineering and quantum information technology. A long-standing goal in photonics is to integrate on-chip semiconductor laser sources with nonlinear optical components. Engineering waveguide lasers with spectra that phase-match to nonlinear processes on the same device is a formidable challenge. Here, we demonstrate difference-frequency generation in an AlGaAs Bragg reflection waveguide which incorporates the gain medium for the pump laser in its core. We include a quantum dot layer in the AlGaAs waveguide that generates electrically driven laser light at ~ 790 nm, and engineer the structure to facilitate nonlinear processes at this wavelength. We perform difference-frequency generation from 1540 nm to 1630 nm using the on-chip laser, which is enabled by the broad modal phase-matching of the AlGaAs waveguide, and measure conversion efficiencies up to $(7.5 \pm 2.4) \cdot 10^{-2} \%$ /W/cm². Our work paves the way towards devices unifying on-chip active elements and strong optical nonlinearities to enable highly integrated photonic systems-on-chip.

Second-order ($\chi^{(2)}$) nonlinear optical processes [1, 2] have been widely utilized in quantum computation, communication and metrology [3–11]. In addition, second-harmonic (SHG), difference-frequency (DFG) and sum-frequency generation, can be used to prepare and measure ultrafast laser pulses [12, 13], erase spectral distinguishability between single photon emitters [14] and engineer lasers at otherwise hard-to-reach wavelengths [15]. Today, most $\chi^{(2)}$ photonic devices rely on crystals such as BaB₂O₄, LiNbO₃ or KTiOPO₄ that are limited in scalability as they cannot directly host active optical components such as lasers and photodetectors.

Photonic circuits in the direct band-gap semiconductor AlGaAs enable integration of active components on a platform with strong $\chi^{(2)}$ nonlinearity $d_{\text{eff}} \approx 119$ pm/V [16]. Significant effort has been committed to develop miniaturized, on-chip AlGaAs devices with increasing complexity and richer applications [17–19]. In particular, AlGaAs Bragg-reflection waveguides (BRWs) facilitate phase-matching in the telecom band and exhibit strong mode confinement, which has led to comparatively large nonlinear conversion efficiencies up to $2.5 \cdot 10^{-2} \%$ /W/cm² for DFG [20]. Simple waveguide circuits [21], entangled photon pair sources [22, 23], single photon emitters [24] and on-chip lasers [25] have been demonstrated with BRWs. However, there has been limited development of devices that exploit active components, such as lasers, and the strong second order nonlinearity at the same time [26, 27].

In this work, we demonstrate an AlGaAs BRW with an embedded quantum dot (QD) laser at ~ 790 nm wavelength that is engineered to emit in the Bragg mode. The

nonlinear waveguide thereby comprises the active gain medium in an edge-emitting cavity, forming our electrically driven pump laser. We determine the threshold current of the internal laser and use the chip temperature to tune its spectral properties, such that it fulfills the requirements to pump type-2 nonlinear processes. By injecting a telecom signal laser into this nonlinear cavity, we generate an additional telecom idler field via DFG. We reconstruct the joint spectral intensity (JSI) by measuring the generated idler field, and extract a nonlinear conversion efficiency of up to $(7.5 \pm 2.4) \cdot 10^{-2} \%$ /W/cm², which is on-par with previously reported BRWs without internal laser (passive structures).

We fabricate our BRWs starting with an epitaxially grown Al_xGa_{1-x}As stack with varying aluminum concentrations x and layer thicknesses [28]. We subsequently pattern waveguides by electron beam lithography and dry etching in Ar and Cl₂ plasma. In this work, we utilize a 1.48 mm long and 3.5 μ m wide waveguide sample, for which a schematic is depicted in Fig. 1. The device is planarized with Benzocyclobutene (BCB) to allow for depositing electrical contact pads larger than the waveguide width. The layer structure enables modal phase-matching between the fundamental, total internal reflection mode at ~ 1580 nm confined to the core and matching layers, and higher order Bragg modes at ~ 790 nm confined by the Bragg-mirror stacks [29, 30]. In our device, a layer of Al_{0.13}In_{0.47}Ga_{0.4}As QDs is embedded at the center of the waveguide core and is surrounded by a AlGaAs quantum well to increase carrier accumulation. We dope the upper and lower mirror stacks as well as the substrate with carbon and silicon atoms to create a p-i-n junction. The mechanically cleaved waveguide facets have $\sim 30 \%$ reflectivity and form a cavity surrounding the gain medium. The QD dipoles are oriented to emit horizontally polarized

* alexander.schlager@uibk.ac.at

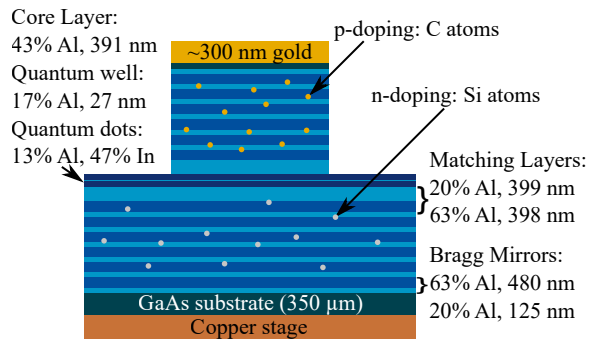


FIG. 1. Schematic of the waveguide cross section. The QDs are embedded within a 27 nm thin quantum well layer, which is centered in the core. The light is vertically confined by the Bragg mirrors and together with an external signal laser is converted to telecom wavelengths.

light into the Bragg mode.

We use a pulsed voltage supply to characterize the QD laser with 0.4% duty cycle (8 kHz repetition rate, 500 ns pulse width) to reduce the thermal load on the sample while still achieving peak currents above the lasing threshold. We increase the peak voltage of the pulse generator and measure the current and generated optical power. This way, we determine the lasing threshold of (618 ± 4) mA, which corresponds to a current density of (11.9 ± 0.5) kA/cm², as can be seen in Fig. 2. The insets depict the spectrum of the laser below and above the threshold current, respectively. This result is comparable to similar integrated lasers in BRWs [26], however, structures optimized only for lasing can offer significantly lower lasing thresholds down to a few tens of milliamperes [25, 27]. Temperature can be used to tune the laser spectrum as it modifies the material band-gap and refractive index. In Fig. 3a) we plot the spectrum versus temperature from 0 °C to 10 °C which enables tuning from 789 nm to 793 nm. The large spectral jumps of ~ 2 nm have been observed previously [26] and are caused by saturable absorption within AlGaAs laser structures [31, 32].

In addition to the introduction of an internal QD laser, we engineer our BRWs to achieve modal phase-matching between the Bragg mode at ~ 790 nm and the total internal reflection mode at ~ 1580 nm to enable second-order nonlinear optical processes. The nonlinear frequency conversion obeys energy and momentum conservation

$$\omega_p = \omega_s + \omega_i \quad (1)$$

$$k_p(\omega_p) = k_s(\omega_s) + k_i(\omega_i), \quad (2)$$

where ω_j and $k_j(\omega_j) = n_j\omega_j/c$ are the frequency and wavenumber with $j \in \{p, s, i\}$ corresponding to pump, signal and idler. The wavenumbers are directly proportional to the effective refractive indices n_j of the corresponding modes and c is the speed of light. Thus, we engineer the effective refractive index of our modes to achieve phase-matching at the desired wavelengths [33].

We initially characterize the phase-matching by per-

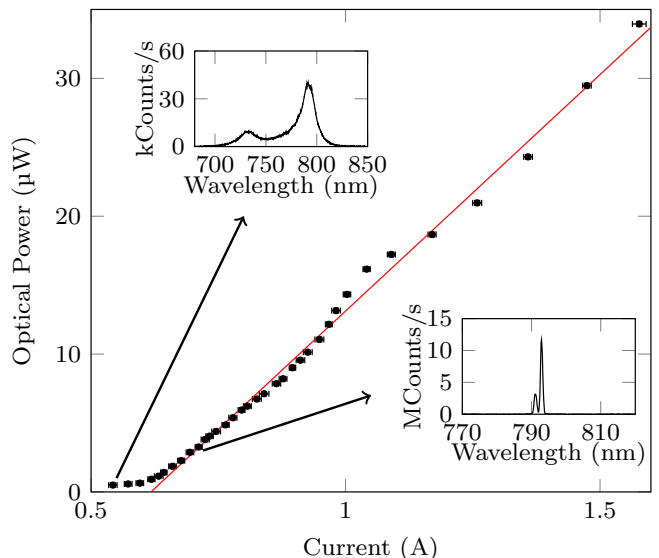


FIG. 2. The optical power of the internal laser for different current settings at 3.5 °C. We use a linear fit starting with the 6th data point, which results in a threshold of (618 ± 4) mA. The insets depict the measured spectra at about 540 mA and 700 mA respectively.

forming SHG with an external telecom laser. We investigate the SHG spectrum for each type of nonlinear process by scanning the telecom laser wavelength and controlling the input and output polarization with half-wave plates and polarizers. We also use temperature to tune the phase-matching wavelength and plot the recorded central up-converted wavelengths in Fig. 3b). Our BRWs exclusively produce horizontally polarized output by type-2 SHG, which means the quantum dot laser can only pump the corresponding DFG process. We find a working point for electrically pumped operation at 3.5 °C, at which the spectra of the laser and type-2 process overlap, as can be seen in Figs. 3c) and d). The spectrum of the laser can be slightly tuned by fine adjustment of the temperature and current. This way, we are able to shift the intensity maximum from 791 nm to 792.9 nm, as shown in Fig. 3c). However, increasing the current by more than a few mA causes the central wavelength of the laser to shift away from the phase-matching wavelength. Therefore, we can only operate in a low-current regime and access ~ 3 μW of laser power while maintaining the high spectral overlap. Adjusting the phase-matching wavelength or laser spectrum by a few nanometers in future structures, by modifying the layer thicknesses or quantum dot composition, could enable at least a tenfold increase in the usable laser power.

Now that we know the conditions necessary for the QD laser spectrum and phase-matching to overlap, we can investigate DFG. We initially use an external laser to verify the type-2 DFG process, before turning to the internal QD laser. We utilize the setup shown in Fig. 4a), where we use half-wave plates and a polarizer to control

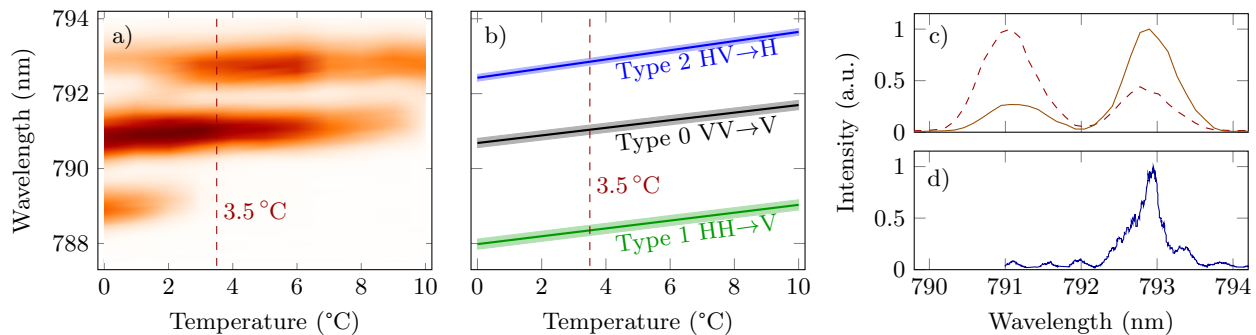


FIG. 3. a) Temperature dependence of the internal quantum dot laser spectrum. b) Temperature dependence of the type 0 (black), type I (green) and type II (blue) SHG signal. The thick lines are linear fits of the measured central wavelengths and the bands indicate their standard deviation. c) Spectra of the internal laser at 3.5 °C with two slightly different driving (peak) currents around 700 mA. The dashed line corresponds to the spectrum in a) and the solid line to a spectrum optimized for DFG. d) The type 2 second-harmonic-generation signal with its peak at 792.9 nm.

the power and polarization of the pump and seed laser, which are combined at a dichroic mirror and coupled into the waveguide with a 100× microscope objective. The generated idler photons are then collected with a 0.68 NA aspheric lens and coupled to a spectrometer with a high-sensitivity InGaAs CCD. We use polarization, longpass, and bandpass filters to suppress the pump and seed lasers. This is necessary as the seed laser is much stronger than the DFG light, and we are working close to degeneracy, making spectral filtering a challenge.

We characterize the DFG process using the external pump laser set to 14 mW at 792.9 nm and the telecom seed laser set to 13 mW at 1614.0 nm after the microscope objective, which stimulates the corresponding DFG idler emission at 1558 nm as can be seen in Fig. 4b). We repeat this measurement with the internal QD laser as the pump, which produces the result shown in Fig. 4c). Note that the 0.4% duty cycle of the pulse generator results in a reduced intensity of the idler field by a factor of 250. For both cases, we tune the seed laser wavelength from 1530 nm to 1640 nm to measure the JSI – the correlation of signal (seed) and idler (DFG) wavelengths – which is enabled by the broad phase-matching of the BRW. The JSIs for the external and internal pump lasers are shown in Figs. 4d) and e). Close to degeneracy ($\lambda_s \approx \lambda_i$), we can no longer fully suppress the seed laser, and therefore cannot measure the DFG spectrum. For the external laser, we are not able to record the idler emission beyond ~ 1620 nm due to reduced detector efficiency. However, we can circumvent this limitation with the internal QD laser by changing the polarization of the seed laser to vertical. This way, we seed the idler mode above ~ 1620 nm and measure the signal mode that is generated by DFG. This technique is not possible for the external laser as we set both pump and seed to horizontal polarization with a single polarizer.

Finally, we investigate the nonlinear conversion efficiency of our BRWs. We use the same settings as before, but fix the seed laser wavelength while tuning its power.

This way, we measure the power dependency of the integrated DFG spectrum, as shown in Figs. 4f) and g) for the external and internal laser, respectively. By adding a linear fit, we extract the slope b in units of Hz/mW and the offset, which corresponds to the constant background (i.e. photoluminescence, dark counts and stray light). Note that we have chosen to tune the seed power since photoluminescent background light [34] is not promoted by telecom wavelengths and is thus a constant in our measurement. We determine the conversion efficiency

$$\eta_{\text{conv}} = \frac{n}{\eta_{\text{setup}}} \frac{P_i}{P_s P_p L^2} = \frac{n}{\eta_{\text{setup}}} \frac{b E_\gamma}{P_p L^2}, \quad (3)$$

where P_p , P_s and P_i are the average powers of the pump, signal and idler beams, respectively, $L = 1.48$ mm is the waveguide length and E_γ is the energy of the frequency converted photons. The number of photons needed to register one count in the spectrometer $n = (2.4 \pm 0.4) \cdot 10^4$ takes into account any losses caused by fiber matings, and coupling into the spectrometer, as well as the detection efficiency of the camera. Furthermore, we normalize the result for the setup efficiency $\eta_{\text{setup}} = 14.74\%$ for telecom light, which includes the transmission of all optical elements and fiber coupling (see Appendix 2 for a detailed list of efficiencies). For the external pump laser, the power is set to $P_p = 14$ mW after the microscope objective and for the internal QD laser, the power is set to $P_p = 2.9 \mu\text{W}$ after the aspheric lens. We extract the conversion efficiencies $(1.1 \pm 0.2) \cdot 10^{-3} \%$ /W/cm² and $(7.5 \pm 2.4) \cdot 10^{-2} \%$ /W/cm² for the external and internal pump, respectively, and summarize the results in Table I. We measure approximately 70 times higher conversion efficiency when using the QD laser, however, these values do not include any waveguide propagation or in-coupling losses for the external pump laser. Previous experiments [35] indicate that only 4% to 8% of the external pump laser couples into the Bragg mode, while the internal laser emits almost entirely into this mode (see Appendix 2). Furthermore, the pump and seed lasers

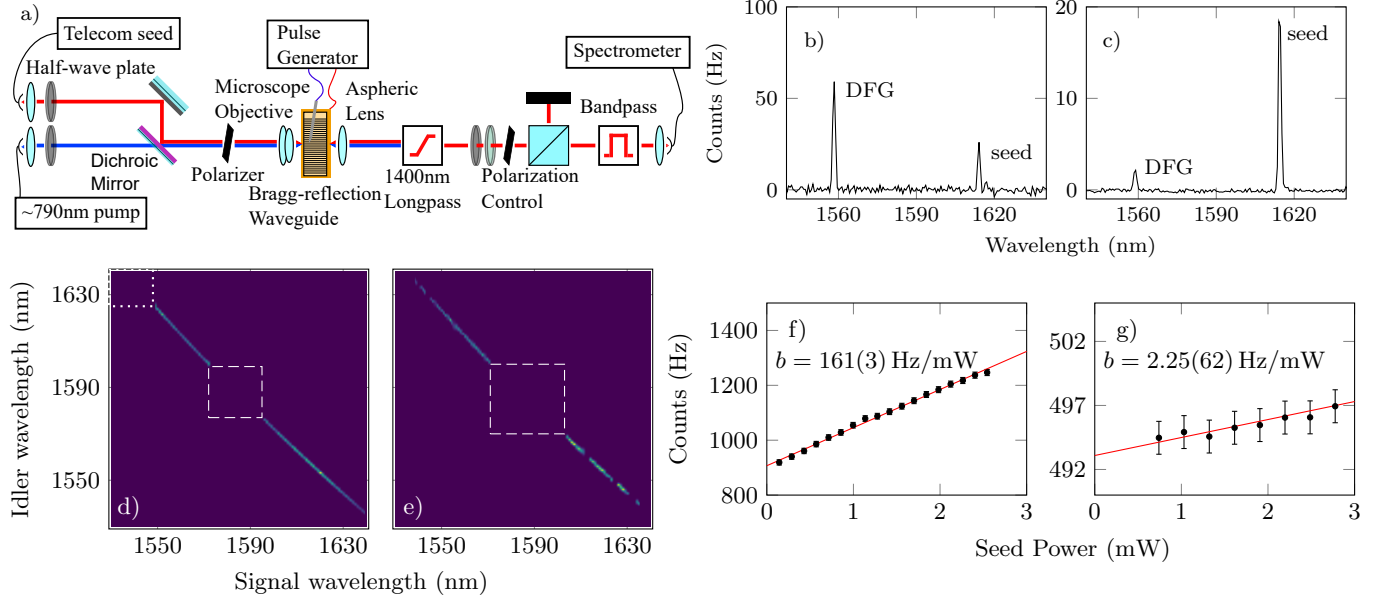


FIG. 4. a) Experimental setup for performing difference frequency generation with the external and internal pump laser. The input lasers are coupled to the waveguide using a microscope objective. After the waveguide, we suppress the pump laser via a 1400 nm longpass filter and the seed laser via polarization control, as well as a bandpass filter. The remaining light is coupled into a single mode fiber and analyzed with a spectrometer and an InGaAs camera at -80°C . Instead of the external pump, an electric pulse generator can be used to drive the internal QD laser. b), c) Examples for the measured DFG spectrum at a seed wavelength of 1614 nm and a pump wavelength of 792.9 nm for b) the external laser and c) the quantum dot laser. Here, the seed laser is set to 1614 nm and the corresponding DFG signal is centered around 1558 nm. d), e) Joint spectral intensity reconstructed via DFG using d) an external laser and e) the internal laser set to a wavelength of 792.9 nm. At the regions marked with a white box, no signal could be measured due to a low detector efficiency (dotted) or insufficient filtering (dashed). f), g) Dependency of the DFG signal on the seed laser power, utilizing the f) external laser and g) the internal laser.

TABLE I. Conversion efficiencies for different measurement settings, using the external and internal laser.

type	λ_p	λ_s (nm)	λ_i (nm)	b (Hz/mW)	$\eta_{\text{conv}}(\%/W/\text{cm}^2)$	corrected $\eta_{\text{conv}}(\%/W/\text{cm}^2)$
internal laser	792.9	1626	1548	2.25 ± 0.62	$(7.5 \pm 2.4) \cdot 10^{-2}$	-
external laser	792.9	1619	1554	161 ± 3	$(1.1 \pm 0.2) \cdot 10^{-3}$	$(5.5 \pm 1.0) \cdot 10^{-2}$
passive sample	767.3	1510	1560	$(10.48 \pm 0.02) \cdot 10^3$	$(5.3 \pm 0.9) \cdot 10^{-2}$	2.7 ± 0.5

cannot be focused equally well by the microscope objective because of chromatic aberration, leading to reduced coupling efficiency into the waveguide. Normalizing for this additional loss, we obtain a conversion efficiency of $(5.5 \pm 1.0) \cdot 10^{-2} \%/W/\text{cm}^2$ for the external laser, which is comparable to the internally pumped result. In fact, we would expect the conversion efficiencies to be the same, as all differences are taken care of in Eq. (3).

As a comparison, we perform DFG using a similar BRW, but without the QD layer or doping and with comparable phase-matching wavelengths. For this, we use the external laser set to 15 mW at 767.3 nm and the seed laser set to 1510 nm in the same experimental setup, which yields a conversion efficiency of $(5.3 \pm 0.9) \cdot 10^{-2} \%/W/\text{cm}^2$ for a DFG emission at 1560 nm. This value is about a factor of 50 higher than the active sample when using the external pump, which is a result of the lower waveguide losses and stronger effective nonlinearity of this device. Hence, with

further engineering to reduce losses and improve the mode overlap, we expect the active structure to achieve at least an order of magnitude higher conversion efficiency.

Adding a reflective coating to the waveguide facets would improve the laser cavity and decrease the lasing threshold. Combined with thicker gold contacts, this could enable DC pumping, i.e. CW operation. We believe that further engineering of the AlGaAs layer thicknesses, material composition and doping will increase the overall performance of the device significantly [28]. Optical powers on the order of a few milliwatts have already been observed in comparable BRWs, which were optimized for lasing [25]. However, it remains a challenge to engineer a structure that is optimal for both lasing and nonlinear frequency conversion.

In conclusion, we have demonstrated an integrated QD laser embedded in an AlGaAs BRW structure. By controlling the temperature of the chip, the internal laser

wavelength can reach the nonlinear phase-matching condition, allowing for electrically pumped nonlinear processes. We have determined the nonlinear conversion efficiency of this sample via DFG, and made a comparison by externally pumping the process and with a passive structure. This device demonstrates a large potential to improve our active chip design, which could facilitate high efficiency on-chip frequency converters. Since DFG uses the same principle and nonlinear effects as SPDC our work presented here marks a significant step towards fully integrated active and nonlinear photonic circuits.

AUTHOR CONTRIBUTIONS

Conceptualization, A.S., R.J.C., S.F., G.W.; Formal analysis, A.S., M.G.; Methodology, A.S., R.J.C., S.F.; Investigation, A.S., M.G.; Resources, H.T., H.S., M.K., S.H., C.S.; Software, A.S., M.G., R.J.C.; Supervision, R.J.C.,

S.F., G.W.; Writing - original draft, A.S., R.J.C.; Writing - review & editing, All Authors; Funding acquisition, C.S., G.W.;

ACKNOWLEDGMENTS

The authors acknowledge funding by the Austrian Science Fund (FWF) under projects Q3 (*IGUANA*), project I2065 and the Special Research Program (SFB) *BeyondC* project no. F7114, the DFG project no. SCHN1376/2-1, the EU H2020 quantum flagship program *UNIQUORN* (Grant No. 820474) and the State of Bavaria. We thank B. Pressl for laboratory assistance.

REFERENCES

-
- [1] R. W. Boyd, *Nonlinear Optics* (Academic Press, 2003).
- [2] A. Christ, B. Brecht, W. Mauerer, and C. Silberhorn, “Theory of quantum frequency conversion and type-II parametric down-conversion in the high-gain regime,” *New Journal of Physics* **15**, 053038 (2013), doi:10.1088/1367-2630/15/5/053038.
- [3] B. G. Christensen, K. T. McCusker, J. B. Altepeter, B. Calkins, T. Gerrits, A. E. Lita, A. Miller, L. K. Shalm, Y. Zhang, S. W. Nam, N. Brunner, C. C. W. Lim, N. Gisin, and P. G. Kwiat, “Detection-loophole-free test of quantum nonlocality, and applications,” *Phys. Rev. Lett.* **111**, 130406 (2013), doi:10.1103/PhysRevLett.111.130406.
- [4] J. L. O’Brien, “Optical quantum computing,” *Science* **318**, 1567 (2007), doi:10.1126/science.1142892.
- [5] T. Rudolph, “Why I am optimistic about the silicon-photonics route to quantum computing,” *APL Photonics* **2**, 030901 (2017), doi:10.1063/1.4976737.
- [6] J. L. O’Brien, A. Furusawa, and J. Vučković, “Photonic quantum technologies,” *Nature Photonics* **3**, 687–695 (2009), doi:10.1038/nphoton.2009.229.
- [7] J. H. Shapiro, “The Quantum Illumination Story,” *IEEE Aerospace and Electronic Systems Magazine* **35**, 8–20 (2020), doi:10.1109/MAES.2019.2957870.
- [8] V. Krutyanskiy, M. Meraner, J. Schupp, V. Krcmarsky, H. Hainzer, and B. P. Lanyon, “Light-matter entanglement over 50 km of optical fibre,” *npj Quantum Information* **5**, 1–5 (2019), doi:10.1038/s41534-019-0186-3.
- [9] M. A. Albota and F. N. C. Wong, “Efficient single-photon counting at 1.55 μm by means of frequency upconversion,” *Opt. Lett.* **29**, 1449–1451 (2004), doi:10.1364/OL.29.001449.
- [10] M. Liscidini and J. E. Sipe, “Stimulated emission tomography,” *Phys. Rev. Lett.* **111**, 193602 (2013), doi:10.1103/PhysRevLett.111.193602.
- [11] H.-S. Zhong, H. Wang, Y.-H. Deng, M.-C. Chen, L.-C. Peng, Y.-H. Luo, J. Qin, D. Wu, X. Ding, Y. Hu, P. Hu, X.-Y. Yang, W.-J. Zhang, H. Li, Y. Li, X. Jiang, L. Gan, G. Yang, L. You, Z. Wang, L. Li, N.-L. Liu, C.-Y. Lu, and J.-W. Pan, “Quantum computational advantage using photons,” *Science* **370**, 1460–1463 (2020), doi:10.1126/science.abe8770.
- [12] J. A. Armstrong, “Measurement of picosecond laser pulse widths,” *Applied Physics Letters* **10**, 16–18 (1967), doi:10.1063/1.1754787.
- [13] P. F. Moulton, “Spectroscopic and laser characteristics of $\text{Ti:Al}_2\text{O}_3$,” *Journal of the Optical Society of America B* **3**, 125 (1986), doi:10.1364/JOSAB.3.000125.
- [14] J. H. Weber, B. Kambs, J. Kettler, S. Kern, J. Maisch, H. Vural, M. Jetter, S. L. Portalupi, C. Becher, and P. Michler, “Two-photon interference in the telecom C-band after frequency conversion of photons from remote quantum emitters,” *Nature Nanotechnology* **14**, 23–26 (2019), doi:10.1038/s41565-018-0279-8.
- [15] N. Leindecker, A. Marandi, R. L. Byer, and K. L. Vodopyanov, “Broadband degenerate OPO for mid-infrared frequency comb generation,” *Optics Express* **19**, 6296 (2011), doi:10.1364/OE.19.006296.
- [16] I. Shoji, T. Kondo, and R. Ito, “Second-order nonlinear susceptibilities of various dielectric and semiconductor materials,” *Optical and Quantum Electronics* **34**, 797–833 (2002), doi:10.1023/A:1016545417478.
- [17] L. Chang, W. Xie, H. Shu, Q. F. Yang, B. Shen, A. Boes, J. D. Peters, W. Jin, C. Xiang, S. Liu, G. Moille, S. P. Yu, X. Wang, K. Srinivasan, S. B. Papp, K. Vahala, and J. E. Bowers, “Ultra-efficient frequency comb generation in AlGaAs-on-insulator microresonators,” *Nature Communications* **11**, 1–8 (2020), doi:10.1038/s41467-020-15005-5.
- [18] C. P. Dietrich, A. Fiore, M. G. Thompson, M. Kamp, and S. Höfling, “Gaas integrated quantum photonics: Towards compact and multi-functional quantum photonic integrated circuits,” *Laser Photon Rev.* **10**, 870 (2016), doi:10.1002/lpor.201500321.
- [19] A. Orioux, M. A. Versteegh, K. D. Jöns, and S. Ducci, “Semiconductor devices for entangled photon pair generation: A review,” *Reports on Progress in Physics* **80** (2017), doi:10.1088/1361-6633/aa6955.

- [20] P. Abolghasem, Jun-Bo Han, Dongpeng Kang, B. J. Bijlani, and A. S. Helmy, “Monolithic Photonics Using Second-Order Optical Nonlinearities in Multilayer-Core Bragg Reflection Waveguides,” *IEEE Journal of Selected Topics in Quantum Electronics* **18**, 812–825 (2012), doi:10.1109/JSTQE.2011.2135841.
- [21] J. Belhassen, F. Baboux, Q. Yao, M. Amanti, I. Favero, A. Lemaître, W. S. Kolthammer, I. A. Walmsley, and S. Ducci, “On-chip III-V monolithic integration of heralded single photon sources and beamsplitters,” *Applied Physics Letters* **112**, 071105 (2018), doi:10.1063/1.5015951.
- [22] A. Vallés, M. Hendrych, J. Svozilík, R. Machulka, P. Abolghasem, D. Kang, B. J. Bijlani, A. S. Helmy, and J. P. Torres, “Generation of polarization-entangled photon pairs in a Bragg reflection waveguide,” *Opt. Express* **21**, 10841 (2013), doi:10.1364/OE.21.010841.
- [23] A. Schlager, B. Pressl, K. Laiho, H. Suchomel, M. Kamp, S. Höfling, C. Schneider, and G. Weihs, “Temporally versatile polarization entanglement from Bragg reflection waveguides,” *Opt. Lett.* **42**, 2102 (2017), doi:10.1364/OL.42.002102.
- [24] K. D. Jöns, U. Rengstl, M. Oster, F. Hargart, M. Heldmaier, S. Bounouar, S. M. Ulrich, M. Jetter, and P. Michler, “Monolithic on-chip integration of semiconductor waveguides, beamsplitters and single-photon sources,” *Journal of Physics D: Applied Physics* **48**, 085101 (2015), doi:10.1088/0022-3727/48/8/085101.
- [25] B. Janjua, M. Iu, Z. Y. P. Charles, E. Chen, and A. S. Helmy, “Passively mode-locked Bragg lasers with 64 GHz sub-300 fs pulses at 785 nm,” *IEEE Photonics Technology Letters* **1135**, 1–1 (2020), doi:10.1109/lpt.2020.3013815.
- [26] C. Autebert, G. Maltese, Y. Halioua, F. Boitier, A. Lemaître, M. Amanti, C. Sirtori, and S. Ducci, “Electrically Injected Twin Photon Emitting Lasers at Room Temperature,” *Technologies* **4**, 24 (2016), doi:10.3390/technologies4030024.
- [27] B. J. Bijlani, P. Abolghasem, and A. S. Helmy, “Semiconductor optical parametric generators in isotropic semiconductor diode lasers,” *Appl. Phys. Lett.* **103**, 091103 (2013), doi:10.1063/1.4819736.
- [28] B. Pressl, K. Laiho, H. Chen, T. Günthner, A. Schlager, S. Auchter, H. Suchomel, M. Kamp, S. Höfling, C. Schneider, and G. Weihs, “Semi-automatic engineering and tailoring of high-efficiency Bragg-reflection waveguide samples for quantum photonic applications,” *Quantum Science and Technology* **3**, 024002 (2018), doi:10.1088/2058-9565/aaa2a2.
- [29] P. Abolghasem and A. S. Helmy, “Matching Layers in Bragg Reflection Waveguides for Enhanced Nonlinear Interaction,” *IEEE Journal of Quantum Electronics* **45**, 646–653 (2009), doi:10.1109/jqe.2009.2013118.
- [30] B. Pressl, K. Laiho, H. Chen, T. Günthner, A. Schlager, S. Auchter, H. Suchomel, M. Kamp, S. Höfling, C. Schneider, and G. Weihs, “Semi-automatic engineering and tailoring of high-efficiency Bragg-reflection waveguide samples for quantum photonic applications,” *Quantum Sci. Technol.* **3**, 024002 (2017), doi:10.1088/2058-9565/aaa2a2.
- [31] J. Copeland, “Single-mode stabilization by traps in semiconductor lasers,” *IEEE Journal of Quantum Electronics* **16**, 721–727 (1980), doi:10.1109/JQE.1980.1070571.
- [32] N. Chinone, T. Kuroda, T. Ohtoshi, T. Takahashi, and T. Kajimura, “Mode-hopping noise in index-guided semiconductor lasers and its reduction by saturable absorbers,” *IEEE Journal of Quantum Electronics* **21**, 1264–1270 (1985), doi:10.1109/JQE.1985.1072788.
- [33] A. S. Helmy, P. Abolghasem, J. Stewart Aitchison, B. J. Bijlani, J. Han, B. M. Holmes, D. C. Hutchings, U. Younis, and S. J. Wagner, “Recent advances in phase matching of second-order nonlinearities in monolithic semiconductor waveguides,” *Laser Photonics Rev.* **5**, 272 (2011), doi:10.1002/lpor.201000008.
- [34] S. Auchter, A. Schlager, H. Thiel, K. Laiho, B. Pressl, H. Suchomel, M. Kamp, S. Hoefling, C. Schneider, and G. Weihs, “Understanding photoluminescence in semiconductor bragg-reflection waveguides,” *Journal of Optics* (2021), doi:10.1088/2040-8986/abd888.
- [35] B. Pressl, T. Günthner, K. Laiho, J. Gefler, M. Kamp, S. Höfling, C. Schneider, and G. Weihs, “Mode-resolved Fabry-Perot experiment in low-loss Bragg-reflection waveguides,” *Opt. Express* **23**, 33608 (2015), doi:10.1364/OE.23.033608.

APPENDICES

1. Setup used for SHG and laser characterization

The setup used to characterize the internal laser and the SHG within our BRWs is shown in Fig. A1. During the measurements either the telecom laser or the electric pulse generator was turned off, respectively.

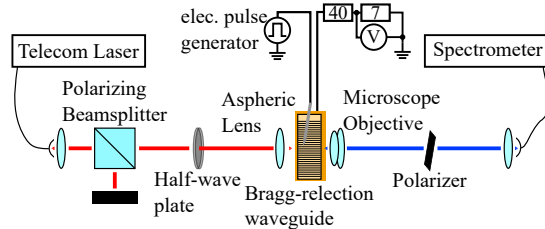


FIG. A1. Experimental setup for characterizing the internal quantum dot laser and SHG spectra. We measure the SHG with the spectrometer by using the telecom laser and collecting the generated photons via the microscope objective. We explore all three types of SHG by adjusting the half-wave plate and polarizer settings. By turning on the electric pulse generator instead, we investigate the properties of the internal quantum dot laser. We determine the peak currents by measuring the voltage with an oscilloscope at a 7Ω resistance.

2. Conversion efficiency correction

To be able to compare our results to similar structures, we have to correct the conversion efficiency for losses caused by the experimental setup, which are listed in Tab. A1. The external laser powers are measured before the microscope objective and corrected for its transmission at the utilized pump wavelength. An internal pump power of $2.8 \mu\text{W}$ is measured after the aspheric lens. Including the transmission of the lens (70%) and the portion of the multi-modal spectrum at the correct wavelength (72%, see Fig. 3c), the power only slightly increases to $P_p = 2.9 \mu\text{W}$.

The idler photons get collected by the aspheric lens (95%) and pass through the polarization control and filters. All elements are coated for optimal transmission in the telecom wavelength range. Nonetheless, only 70% of the light reaches the bandpass filter. The filter is centered at 1540 nm with a bandwidth of 40 nm and its transmission at the generated wavelengths is 75%. After passing the filter, the light is coupled into a polarization maintaining single mode fiber. Due to the shape of the TIR mode, only about 30% of the light can be coupled into the fiber. We include all further fiber mating, spectrometer and detection losses in the photon number $n = (2.4 \pm 0.4) \cdot 10^4$ needed to produce a count on the InGaAs line camera, which is cooled to -80°C to reduce noise.

As we want to compare the externally and internally pumped DFG, we also correct for the mode mismatch of the pump laser and the Bragg mode. As discussed in previous work [35], only about 4% of the pump light propagates in the correct mode. Furthermore, the external pumping requires two lasers with a large spectral separation to be coupled into the waveguide at the same time. This causes another decrease in efficiency, which we estimate to be about 50%. However, this does not affect the internal laser. We believe that most of the internal laser light is coupled in the correct Bragg mode, as depicted in Fig. A2.

TABLE A1. Overview of the correction factors used to determine the conversion efficiency. These values differ only very slightly for the various wavelengths used in the experiments.

	External	Internal	Passive
Power in front of the waveguide	14.2 mW	2.9 μW	11.55 mW
Photons per count n	$(2.4 \pm 0.4) \cdot 10^4$	$(2.4 \pm 0.4) \cdot 10^4$	$(2.4 \pm 0.4) \cdot 10^4$
Filter	75 %	75 %	75 %
Aspheric lens (telecom)	95 %	95 %	95 %
Other Optics	70 %	70 %	70 %
Fiber-Coupling	30 %	30 %	30 %
Mode overlap	4 %	-	4 %
Focus mismatch	50 %	-	50 %

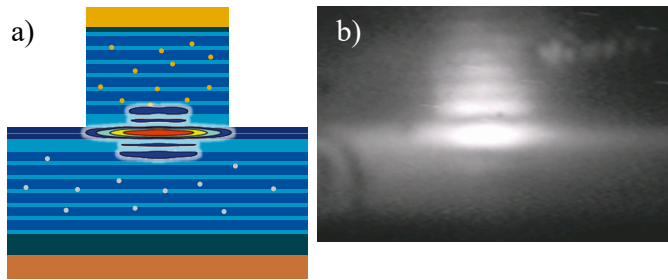


FIG. A2. a) Schematic of the simulated Bragg mode profile and b) recorded internal laser mode profile.

3. Further DFG results

In addition to the previously shown data, we record the conversion efficiency of our active samples at different seed laser wavelengths, as can be seen in Tab. A2. The results show that our BRWs allow for consistent frequency conversion with a wavelength range of at least 20 nm. Hence, within a wavelength region of at least 20 nm our BRW allows for consistent frequency conversion. Analyzing the recorded joint spectral intensity, we expect this regime to be at least 80 nm wide. However, to access the DFG light near the degeneracy, the broad bandpass filter would have to be exchanged by a narrow and tunable one.

TABLE A2. Conversion efficiencies for different measurement settings, using the external and internal laser.

type	λ_p	λ_s (nm)	λ_i (nm)	b (Hz/mW)	$\eta_{\text{conv}}(\%/W/cm^2)$	corrected $\eta_{\text{conv}}(\%/W/cm^2)$
internal laser	792.9	1607	1565	0.92 ± 0.57	$(3.0 \pm 1.9) \cdot 10^{-2}$	-
		1614	1558	1.40 ± 0.57	$(4.6 \pm 2.0) \cdot 10^{-2}$	-
		1619	1554	0.69 ± 0.52	$(2.3 \pm 2.1) \cdot 10^{-2}$	-
		1626	1548	2.25 ± 0.62	$(7.5 \pm 2.4) \cdot 10^{-2}$	-
external laser	792.9	1607	1565	54 ± 3	$(3.6 \pm 0.6) \cdot 10^{-4}$	$(1.8 \pm 0.3) \cdot 10^{-2}$
		1614	1558	139 ± 3	$(9.2 \pm 1.6) \cdot 10^{-4}$	$(4.6 \pm 0.8) \cdot 10^{-2}$
		1619	1554	161 ± 3	$(1.1 \pm 0.2) \cdot 10^{-3}$	$(5.5 \pm 1.0) \cdot 10^{-2}$
		1626	1548	141 ± 3	$(9.5 \pm 1.6) \cdot 10^{-4}$	$(4.8 \pm 0.8) \cdot 10^{-2}$
passive sample	767.3	1510	1560	$(10.48 \pm 0.02) \cdot 10^3$	$(5.3 \pm 0.9) \cdot 10^{-2}$	2.7 ± 0.5